Impact of Defects and Crystal Size on Negative Gas Adsorption in DUT-49 Analyzed by in Situ 129Xe NMR Spectroscopy

Krause, Simon; Reuter, Florian S.; Ehrling, Sebastian; Bon, Volodymyr; Senkovska, Irena; Kaskel, Stefan; Brunner, Eike

Published in:
Chemistry of Materials

DOI:
10.1021/acs.chemmater.0c01059

Publication date:
2020

CHEMISTRY OF MATERIALS

pubs.acs.org/cm

Article

Impact of Defects and Crystal Size on Negative Gas Adsorption in DUT-49 Analyzed by *In Situ* ^{129}Xe NMR Spectroscopy

Simon Krause,* Florian S. Reuter, Sebastian Ehrling, Volodymyr Bon, Irena Senkovska, Stefan Kaskel,* and Eike Brunner*

Cite This: *Chem. Mater.* 2020, 32, 4641−4650

Read Online

ACCESS | Metrics & More | Article Recommendations | Supporting Information

ABSTRACT: The origin of crystal-size-dependent adsorption behavior of flexible metal−organic frameworks is increasingly studied. In this contribution, we probe the solid−fluid interactions of DUT-49 crystals of different size by *in situ* ^{129}Xe NMR spectroscopy at 200 K. With decreasing size of the crystals, the average solid−fluid interactions are found to decrease reflected by a decrease in chemical shift of adsorbed xenon from 230 to 200 ppm, explaining the lack of adsorption-induced transitions for smaller crystals. However, recent studies propose that these results can also originate from the presence of lattice defects. To investigate the influence of defects on the adsorption behavior of DUT-49, we synthesized a series of samples with tailored defect concentrations and characterized them by *in situ* ^{129}Xe NMR. In comparison to the results obtained for crystals with different size, we find pronounced changes of the adsorption behavior and influence of the chemical shift only for very high concentrations of defects, which further emphasizes the important role of particle size phenomena.

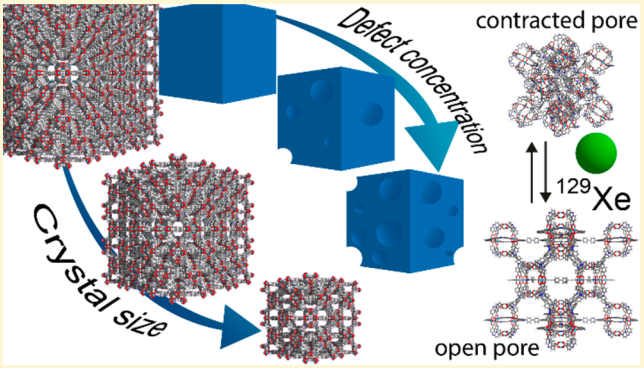

INTRODUCTION

A niche group of metal−organic frameworks (MOFs) are known to undergo large-scale structural transitions upon adsorption and desorption of gases, resulting in unusual adsorption properties.[1] These were found to be beneficial for sensing applications[2,3] as well as storage[4] and separation of gases.[5,6] Often, the complex mechanisms behind structural transitions of these so-called flexible MOFs are elucidated by complex *in situ* investigations.[7] In general, the crystal structures of the different phases and their mixtures observed before and after the transition provide some rationale for understanding the behavior of the "real world" material. However, crystal size and morphology effects are often overlooked considering structural transitions of a periodic crystal structures, but these can drastically impact the materials' properties. In recent years, the number of reports on crystal-size-dependent adsorption behavior of flexible MOFs is increasing. So far, no general mechanism has been postulated due to limited experimental and especially computational analysis.[8,9] Often, empirical correlations are based on analyzing a series of MOF samples for which the synthesis conditions are adopted to yield different crystallite sizes under comparable chemical composition.[10−15] However, the formation of microscopic defects beyond the resolution and accuracy of the applied characterization techniques can impact the adsorption behavior unnoticedly.[16] The potential of formation of lattice defects is in particular important for the usage of modulator agents which impact the crystallization process and consequently the crystal size.[17,18] Often, modulator molecules such as monocarboxylic acids are found to be present in the resulting solids.[19] Thus, several attempts have been undertaken to synthesize flexible MOFs with varying crystal size distribution without using modulators.[10,11,20] However, rapid crystallization can still result in lattice defects. It is thus of crucial interest to further investigate the impact of crystal size and defects on structural transitions in flexible MOFs.

Recently, we reported a novel adsorption phenomenon called negative gas adsorption (NGA) in which the mesoporous MOF DUT-49(Cu) expels gas from the pores upon structural contraction.[21] In previous work, NGA was investigated in detail by a range of *in situ* crystallographic and spectroscopic methods aided by computational investigation.[22] Instead of analyzing structure before and after the transition of the solid, we used *in situ* ^{129}Xe NMR to monitor NGA from the perspective of the guest molecule. ^{129}Xe NMR is a technique

Received: March 10, 2020
Revised: May 10, 2020
Published: May 11, 2020

https://dx.doi.org/10.1021/acs.chemmater.0c01059
Chem. Mater. 2020, 32, 4641−4650

frequently used to study adsorption processes in MOFs[23−25] and other porous solids.[24,26−30] In these experiments, the chemical shift of xenon is monitored as a function of pressure and temperature. In the analysis of DUT-49 an abrupt increase in chemical shift by ca. 100 ppm upon contraction and NGA is observed at a relative pressure of 0.13−0.18 at 200 K, providing a very sensitive technique to detect the structural transition.[31] In addition, this method is particularly suitable for analyzing materials with subtle differences in composition and surface functionality because the chemical shift of xenon is sensitive toward changes in porosity and surface functionality.[32] While analyzing the behavior of DUT-49 upon adsorption of nitrogen at 77 K, we observed a strong dependence of NGA and structural contraction on the crystal size distribution.[33] NGA only occurred in the crystal size range of 2−10 μm while structural contraction was not present in crystals below ca. 2 μm in size. Although the investigated samples showed comparable chemical composition, the impact of potentially undetected defects remained an open question. In this contribution we apply *in situ* ^{129}Xe NMR to analyze the adsorption mechanism in DUT-49 crystals of different size and with different concentrations of defects to answer these open questions.

EXPERIMENTAL SECTION

Synthesis. In this study two sets of samples were prepared (Table 1). First, the impact of crystal size on the adsorption behavior of DUT-49 was investigated by probing the chemical shift of ^{129}Xe, δ, in a wide relative pressure range at 200 K. To cover a wide range of crystal sizes, samples DUT-49(1), -(2), -(3), -(4), and -(5) with mean crystal sizes of 8.7 μm, 4.3 μm, 1.1 μm, 150 nm, and 106 nm, respectively, were investigated. The samples were taken from a previous study, and synthesis conditions and characterization of these materials can be obtained from ref 33. Second, a series of DUT-49 with tailored concentration of defects were synthesized to further investigate the impact of lattice defects on the adsorption behavior of DUT-49. Defects were introduced into the framework of DUT-49 by replacing the tetradentate ligand 9,9′-([1,1′-[biphenyl]-4,4′-diyl)[bis-(9*H*-carbazole-3,6-dicarboxylate (bbcdc) with the structurally related bidentate 9*H*-carbazole-3,6-dicarboxylate (cdc), while maintaining the connectivity of the Cu-SBU and MOP. In a series of solvothermal syntheses the H_2cdc/H_4bbcdc ratio was increased from 0.5 to 200, keeping the Cu to carboxylate ratio to 0.5 (Table S1). The reactions were conducted in NMP at 80 °C for 24 h, yielding blue powders which were analyzed by PXRD (Figure 2). As a control experiment H_2cdc was reacted with copper nitrate in NMP at 80 °C to obtain a potential side product of the reaction. This reaction yielded hexagonal crystals of DUT-158.

Table 1. Definition and Composition of DUT-158 and DUT-49 Samples with Different Crystal Sizes and Number of Defects (def)

material ID	composition	mean crystal size (nm)
DUT-49(1)	$Cu_2(bbcdc)_1$	8750 ± 2620
DUT-49(2)	$Cu_2(bbcdc)_1$	4269 ± 1871
DUT-49(3)	$Cu_2(bbcdc)_1$	1163 ± 968
DUT-49(4)	$Cu_2(bbcdc)_1$	150 ± 80
DUT-49(5)	$Cu_2(bbcdc)_1$	107 ± 71
defDUT-49(0)	$Cu_2(bbcdc)_1$	2041 ± 1213
defDUT-49(1)	$Cu_{2.004}(cdc)_{0.004}(bbcdc)_1$	1778 ± 825
defDUT-49(2)	$Cu_{2.078}(cdc)_{0.078}(bbcdc)_1$	1770 ± 811
defDUT-49(3)	$Cu_{2.24}(L_1)_{0.24}(bbcdc)_1$	1417 ± 776
defDUT-49(4)	$Cu_{2.33}(cdc)_{0.33}(bbcdc)_1$	849 ± 342
defDUT-49(5)	$Cu_{2.98}(cdc)_{0.98}(bbcdc)_1$	n.a.
defDUT-49(6)	$Cu_{3.5}(cdc)_{1.5}(bbcdc)_1$	n.a.
defDUT-49(7)	$Cu_2(bbcdc)_1$	2041 ± 1213
DUT-158	Cu(cdc)	n.a.

General Methods. Synthesis procedures for H_2cdc (9*H*-carbazole-3,6-dicarboxylic acid) and H_4bbcdc (9,9′-(1,1′-[biphenyl]-4,4′-diyl)[bis(9*H*-carbazole-3,6-dicarboxylate)]) can be obtained from refs 34 and 35. ^{1}H Nuclear magnetic resonance (NMR) spectra were acquired on a Bruker Avance III 500 spectrometer (500.13 MHz). All ^{1}H are reported in parts per million (ppm) downfield of TMS and were measured relative to the residual signals of the solvents at 2.54 ppm (DMSO). Diffuse reflectance infrared Fourier transform (DRIFT) spectroscopy was performed on a Bruker VERTEX 70 with a SPECAC Golden Gate DRIFT setup. Prior to the measurement, 2 mg of sample was mixed with 10−15 mg of dry KBr in a mortar and pressed in the DRIFT-cell. Thermogravimetric analysis (TGA) was performed in synthetic dry air by using a NETZSCH STA 409 thermal analyzer at a heating rate of 5 K min^{-1}. Air-sensitive MOF samples were prepared in an Ar-filled glovebox and inserted in the instrument with little exposure to ambient conditions. Powder X-ray diffraction (PXRD) patterns were collected in transmission geometry with a STOE STADI P diffractometer operated at 40 kV and 30 mA with monochromatic Cu Kα_1 (λ = 0.15405 nm) radiation, a scan speed of 30−15 s/step, and a step size of 2θ = 0.1°−2°. The samples were placed between nondiffracting adhesive tape. "As made" samples were analyzed while suspended in DMF. Desolvated samples were prepared under an inert atmosphere. Scanning electron microscopy (SEM) images were taken with secondary electrons in a Hitachi SU8020 microscope using 1.0 kV acceleration voltage and 10.8 mm working distance. The powdered samples were prepared on a sticky carbon sample holder. To avoid degradation upon exposure to air, the samples were prepared under an argon atmosphere. For each sample a series of images were recorded at different magnifications, and for each sample three different spots on the sample holder were investigated. The crystal size refers to the edge length of the cubic crystals as they are the easiest to measure. The analysis of the SEM images was performed with the ImageJ software package, and values for mean crystal size as well as relative standard deviation (RSD) were obtained by using the ImageJ Analyze-Distribution function.[36] Volumetric adsorption experiments were performed on a BELSORP-max instrument, gases with high purity were used (N_2: 99.999%; He: 99.999%), and the measuring routine of BELSORP-max was used. Targeted relative pressures in the range 0.01−100 kPa were defined, and limits of excess and allowance amount were set to 10 and 20 cm^3 g^{-1}, respectively. Equilibration conditions for each point were set to 1% pressure change within 350 s. The dead volume was routinely determined by using helium. Values for the adsorbed amount of gas in the framework are all given at standard temperature and pressure (STP). Liquid nitrogen was used as coolant for measurements at 77 K.

^{129}Xe NMR Experiments. *In situ* high-pressure ^{129}Xe NMR experiments were performed on an Avance 300 spectrometer (Bruker, Karlsruhe, Germany) at 83.02 MHz using a 10 mm HR probe (6 μs pulse length). Experiments were performed using a homemade apparatus allowing sample pressurization directly inside the NMR magnet. The apparatus uses a high-pressure single crystal sapphire tube with a home-designed gas- and vacuum-tight titanium valve.[24] This apparatus can be connected either to a vacuum pump or to an external gas reservoir. Chemical shifts were referenced by measuring the signal of xenon gas inside the tube at various pressures at room temperature and extrapolation to zero pressure chemical shift. The activated sample is placed into the sapphire tube under an argon atmosphere. Afterward, the sample is evacuated under dynamic high vacuum at about 10^{-4} MPa. The sample tube is then mounted into the NMR spectrometer and connected to an outside xenon reservoir equipped with a pressure gauge using a Teflon hose. This allows the sample pressurization *in situ* within the magnet. We are thus able to measure ^{129}Xe NMR spectra under controlled temperature and at the desired pressure. The pressure was measured by using the pressure sensor Heise ST-2H with a HQSC-2 module with ±0.02 MPa

https://dx.doi.org/10.1021/acs.chemmater.0c01059
Chem. Mater. 2020, 32, 4641−4650

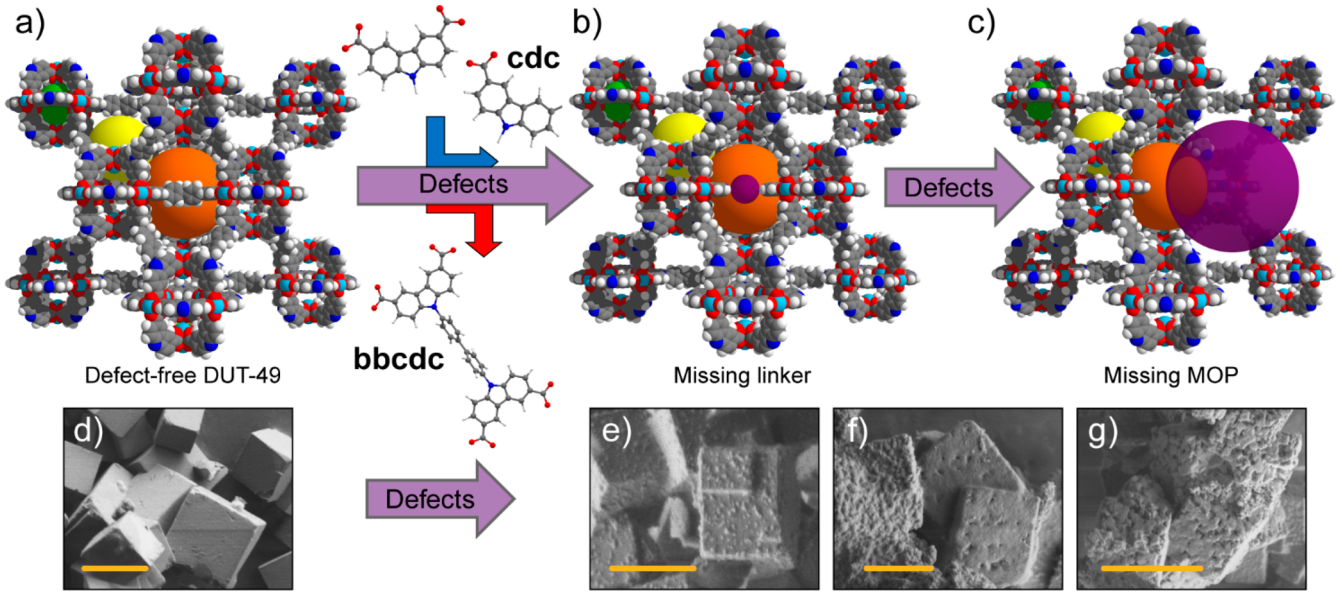

Figure 1. (a–c) Method applied to introduce defects into the DUT-49 lattice by replacement of bbcdc by cdc in the defect free DUT-49 crystal lattice (a) with cdc generating defects (purple) of missing linkers (b) or missing clusters (c). Color code: C, gray; O, red; H, white; N, blue; Cu, turquoise. (d–g) SEM images of defDUT-49(0) (d), defDUT-49(1) (e), defDUT-49(2) (f), and defDUT-49(3) (g); orange scale bar 2 μm.

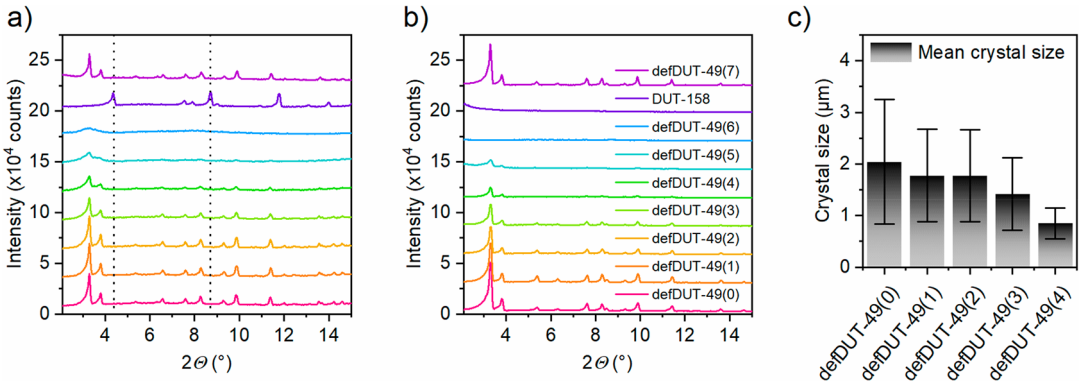

Figure 2. PXRD patterns of defDUT-49 samples and DUT-158 (characteristic peaks indicated as vertical dashed lines) (a) in DMF solvated and (b) desolvated by supercritical activation. (c) Mean crystal size of defDUT-49(0)–(4) determined by SEM analysis.

uncertainty. Samples were allowed to equilibrate for at least 15 min after pressure changes and at least 30 min after temperature changes. ^{129}Xe NMR signals were monitored during this equilibration time to make sure that the signal remains constant after the equilibration period. The sample temperature of 200 K was calibrated following the literature by using the ^{1}H NMR chemical shifts of methanol.[37,38] This method may exhibit systematic errors of a few degrees. The temperature was also calibrated by an independent second method. The condensation pressure of xenon, i.e., the pressure where liquefaction starts inside the tube, was measured at the given temperature. The corresponding temperature was then determined from the phase diagram of xenon with a vapor pressure of xenon at 200 K of 0.52 MPa.

RESULTS AND DISCUSSION

In this study two sets of samples were investigated (Table 1). To monitor the impact of crystal size on the adsorption behavior, samples with mean crystal sizes from 8.7 μm to 106 nm were investigated. To investigate the impact of lattice defects on the adsorption behavior of DUT-49, we decided to rationally introduce defects into the framework of DUT-49 by replacing the tetradentate bbcdc^{4-} by the structurally related bidentate cdc^{2-} ligand. Depending on the concentration of the cdc in the framework, parts of the linker or even whole building blocks such as the MOP will be cleaved (Figure 1). In a control experiment H_2cdc was reacted with copper nitrate to investigate a potential side product of the DUT-49 reaction containing H_2cdc. This reaction yielded hexagonal crystals of DUT-158.

Sample Characterization. First, crystals of DUT-158 were analyzed by PXRD and single crystal diffraction. The crystal structure of DUT-158 consists of 2D layers known for cdc-related ligands (Figure S19).[39] Interestingly, no peaks of DUT-158 and only peaks of the parent DUT-49 structure could be observed in the PXRD patterns of defDUT-49(1)–(6), showing that cdc is incorporated into the DUT-49 lattice (Figure 2). After the powders were washed with DMF, the solvent was exchanged to acetone, which was removed from the pores by supercritical activation protocol previously applied for DUT-49.[34] To remove residual solvent, the samples were degassed in a dynamic vacuum (<10^{-3} kPa) at 100 °C for 24 h. To determine the cdc/bbcdc ratio present in the solids, 10 mg of MOF was dissolved in a mixture of DCl/DMSO-d_6, and ^{1}H NMR spectra were recorded. Comparison of the peak integrals yields the ratio at which the ligands are

https://dx.doi.org/10.1021/acs.chemmater.0c01059
Chem. Mater. 2020, 32, 4641–4650

present in the solid. In general, the amount of cdc implemented into the MOF was in the range of the amount applied in the synthesis (Figure S3). This is well reflected by diffuse reflectance infrared Fourier transform (DRIFT) spectroscopy in which peaks of bbcdc become less pronounced with increasing amount of cdc (Figure S2). Thermogravimetric analysis (Figure S3) shows that the decomposition temperature decreases with increasing cdc content from 300 to 250 °C, indicating that the framework becomes less thermally stable upon introduction of defects. This is well-known for studies performed on defective UiO-66.[40,41]The phase purity of defDUT-49 materials was analyzed by PXRD. In all cases no peaks of DUT-158 could be found, supporting that cdc is implemented into the DUT- 49 lattice and not forming a crystalline side phase (Figure 2). With increasing cdc concentration, broadening of the peaks is observed in both the solvated and desolvated samples, showing that the crystallinity of DUT-49 decreases with increasing concentration of defects. In the case of defDUT-49(6) no peaks are observed after solvent removal, indicating a collapse of the structure. Because the peak broadening could be caused by the formation of small crystals, the morphology and size of the crystals were analyzed by scanning electron microscopy. With increasing cdc content the cubic crystals of DUT-49 are found to be deformed and exhibit holes on the external surface (Figure 1). From the SEM images the crystal size distribution could be determined in which the size represents the edge length of the cubic crystals. With increasing cdc content the mean crystal size is found to decrease from 2 μm (defDUT-49(0)) to 849 nm (defDUT49(4)) (Figure 2). For samples defDUT-49(5) and -(6) no cubic crystals could be detected, and the particles are too small to be further analyzed by SEM (Figure S5). Obviously, the doping with cdc has large effects on the morphology and composition of the crystals of DUT-49. To further determine the impact on the porosity and adsorption behavior, we recorded nitrogen adsorption isotherms at 77 K (Figure S6). With increasing cdc content the total uptake as well as the surface area is found to decrease (Table S3). Furthermore, only samples defDUT-49(0)−(3) exhibit NGA and structural contraction. Isotherms of defDUT-49(4)−(6) exhibit reversible isotherms typical for DUT-49. The absence of hysteresis at higher relative pressures indicates that no additional mesoporosity detectable by N_2 adsorption is generated. Instead, the loss in uptake at higher concentrations of cdc indicates that regions with a high concentration of defects exhibit a collapse of the pore structure. Nevertheless, upon comparison of the normalized isotherms, all materials exhibit the typical type IVb behavior previously found for DUT-49. This indicates that part of the DUT-49 structure is retained even at high concentrations of cdc and potentially embedded in amorphous, nonporous DUT-49 substance. To test whether defects can also be introduced postsynthetically, crystals of defDUT-49(0) were suspended in a 1 M solution of cdc in DMF and heated at 80 °C for 24 h (denoted as defDUT-49(7)). The sample was then washed with fresh DMF, and the solvent was removed analogous to the other samples. NMR analysis showed no presence of cdc in the MOF powder, indicating that postsynthetic ligand exchange in this MOF system cannot be achieved this way while postsynthetic metal exchange is known to occur in DUT-49.[42]

***In Situ* ^{129}Xe NMR Studies of Crystal Size Effects.** In analogy to the previous study of DUT-49, ^{129}Xe NMR spectra were recorded at 200 K and different relative pressures of xenon for samples with different mean crystal size. In the low-pressure region before structural contraction and NGA, all samples follow the same linear trend and exhibit comparable chemical shifts (Figure 3). At a relative pressure of 0.17−0.18

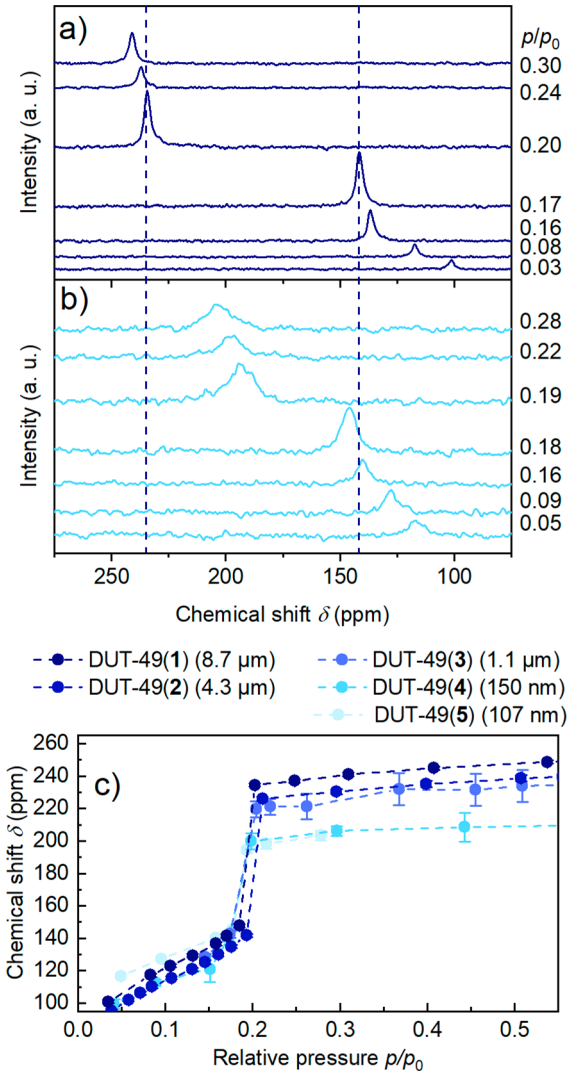

Figure 3. ^{129}Xe NMR spectra of (a) DUT-49(1) (microcrystals) and (b) DUT-49(5) (nanocrystals). Dashed lines represent peak position recorded for DUT-49(1) before (right) and after (left) NGA. (c) Evolution of the chemical shift of Xe at 200 K at increasing relative pressure of Xe for DUT-49 samples with different crystal size distributions.

all samples exhibit NGA and structural contraction indicated by the sudden increase in chemical shift (Figure 3a,b) and increase in pressure in the measuring cell. At a relative pressure of 0.2, that means beyond the pressure of structural contraction, the chemical shift of xenon observed for the five samples shows strong variations. The samples with the smallest crystals DUT-49(5) and -(4) exhibit the lowest chemical shift of 198 ppm. In contrast, samples with increasing crystal size exhibit shifts of 225 to 235 ppm (Figure 3a,b). This trend is maintained up to a relative pressure of 0.7, at which DUT-49(1) and -(2) exhibit a transition from the contracted (*cp*) to the open pore (*op*) structure indicated by the occurrence of a second signal at lower chemical shifts that could previously be assigned to DUT-49*op*.[31] The reduction in chemical shift in

https://dx.doi.org/10.1021/acs.chemmater.0c01059
Chem. Mater. 2020, 32, 4641−4650

the relative pressure range 0.2−0.6 cannot be assigned to an *op*/*cp* mixture which would appear as a peak splitting in the spectra, not observed in the conducted experiments. Consequently, the observed trend for the chemical shift in this pressure range must be a consequence of the different crystal size distributions. What is the origin of these differences in chemical shift, and why is this difference not observed at lower relative pressure <0.2 before structural contraction?

The chemical shift of xenon observed in the performed NMR experiments represents the average of solid−fluid (s-Xe) and fluid−fluid (Xe−Xe) interactions. The latter depend on the density of the fluid, ρ_{Xe}, and the chemical shift can be written as defined by eq 1.

$$\delta = \delta_{s\text{-}Xe} + \delta_{Xe-Xe}(\rho_{Xe}) \quad (1)$$

While solid−fluid interactions are restricted to the interaction with the internal and external surface of the solid, fluid−fluid interactions occur inside the pore, close to the outer surface and also in the interparticular void. The contribution of fluid−fluid interactions increases proportional to the density of xenon. At lower relative pressures (<0.2) the pores in DUT-49*op* are only partially filled with xenon, and the majority of xenon is adsorbed on the inner surface. Thus, solid−fluid interactions dominate the chemical shift. Upon contraction, both the solid−fluid and the fluid−fluid interactions increase drastically because the pores in DUT-49*cp* are suddenly completely filled, and the smaller pore diameter increases the average interaction with the surface. This can be observed by the strongly different chemical shift of DUT-49*op* and *cp* in DUT-49(1) at slightly higher relative pressure. However, the major contributions to the chemical shift originate from the increase in density and consequently enhanced xenon−xenon interactions upon contraction. At 200 K and pressures below saturation, the bulk phase of xenon is gaseous with a much lower density compared to adsorbed xenon. Thus, the chemical shift of gaseous xenon is much lower compared to xenon in the adsorbed phase.[43]

For small particles, one has to consider the possibility of fast exchange between adsorbed xenon inside the particles and xenon outside the particles. In NMR spectra of exchanging systems, the relevant time scale is related to a so-called critical time constant, τ_{crit}, for a two-site exchange between site A and B; the critical time constant can be defined as

$$\tau_{crit} = \frac{1}{2\pi\Delta\nu} \quad (2)$$

where $\Delta\nu = |\nu_A - \nu_B|$ denotes the frequency difference between the two sites. The frequency difference can be calculated as the chemical shift difference between A and B multiplied by the resonance frequency of the respective nucleus at the given magnetic field. If a process is much faster, the considered NMR parameter (e.g., the chemical shift) will be averaged along the trajectory of the process. The same holds in principle if the process includes exchange of xenon between more than two sites: $\Delta\nu$ is then the maximum frequency difference along the trajectory in the porous crystal. The mean residence time, τ_{mean}, of xenon inside a porous crystal depends on two quantities: (i) the self-diffusion coefficient, D, inside the pore system of the crystal, which is impacted by temperature, pressure, pore diameter, and binding energy (adsorption enthalpy), and (ii) the mean crystal diameter d_{cryst}. Because the experiments were conducted at the same temperature, in the same pressure range, and with the same porous material that exhibits uniform ordered porosity, τ_{mean} is mainly influenced by d_{cryst}. The size of τ_{mean} in the pore system ando of the residence time in the surrounding gas phase, τ_{gas}, will determine the average chemical shift, δ, of xenon in fast exchange between the outer crystal surface, the internal porosity of the crystal, and the surrounding gas phase:

$$\delta = P_{ads}\delta_{ads} + P_{gas}\delta_{gas} \quad (3)$$

The probability of being in the adsorbed phase, P_{ads}, is defined as

$$P_{ads} = \frac{N_{ads}}{N_{ads} + N_{gas}} \quad (4)$$

where N_{ads} and N_{gas} are the amount of xenon in the adsorbed and gas phase, respectively, and $P_{gas} = 1 - P_{ads}$. Consequently, the equilibrium between adsorbed and gas phase, which determines the mean residence time in these two phases, will determine the measured chemical shift.

The self-diffusion of xenon in the gas phase at 200 K[44] is fast at the NMR time scale. Consequently, τ_{gas} and also τ_{mean} are short, and the measured chemical shift is expected to represent a weighted average along the trajectory. Crystal downsizing will decrease the mean residence time and consequently P_{ads} of xenon in the adsorbed phase in a single crystal of DUT-49. In addition, in smaller particles the ratio between external and internal surface is increased. It was shown that external surfaces exhibit reduced solid−fluid interactions upon adsorption of gases in ZIF-8,[12] which is expected to be the case for DUT-49 as well. These factors are the origin for the decrease in the experimentally observed chemical shift and in signal intensity with decreasing crystal size (Figure 3). A decrease in P_{ads} would also be reflected by a decrease in uptake in the volumetric adsorption isotherm, which is observed for these samples upon adsorption of nitrogen at 77 K.[45] Interestingly, the decrease in chemical shift for smaller crystals is only observed for the xenon-filled DUT-49*cp* phase and the *op* phase at higher pressures but not for the DUT-49*op* phase at lower pressure before structural transition. At low relative pressure, the degree of pore filling in the *op* phase is rather low, and the amount adsorbed is only slightly influenced by differences in crystal size. This behavior has been previously observed upon nitrogen adsorption in DUT-49[33] and was also reported by Tanaka et al. on ZIF-8.[12] Consequently, diffusivity and host−guest interactions are expected to be less influenced by particle size effects at lower pressures and pore fillings.[30] At higher degrees of pore filling and higher pressures, the self-diffusivity of xenon within the pores is reduced by the increasing density of the fluid. This is the case upon structural contraction and NGA where the xenon density increases significantly due to the shrinkage in pore volume. However, upon structural contraction, d_{cryst} of each crystal is reduced by ca. 22%, which further reduces P_{ads}. Thus, the investigated samples are found to exhibit pronounced differences in chemical shift in the *cp* phase. Because the same observation can be made for xenon adsorbed in the saturated *op* phase at elevated pressures, the observed changes in chemical shift are obviously independent of the crystal structure and truly reflect the solid−fluid and fluid−fluid interactions as well as P_{ads}. This analysis clearly demonstrates that the average adsorption interaction energy is reduced with decreasing crystal size due to decreasing P_{ads} of xenon in a single crystallite. As a result, the adsorption-induced stress and driving force for the

https://dx.doi.org/10.1021/acs.chemmater.0c01059
Chem. Mater. 2020, 32, 4641−4650

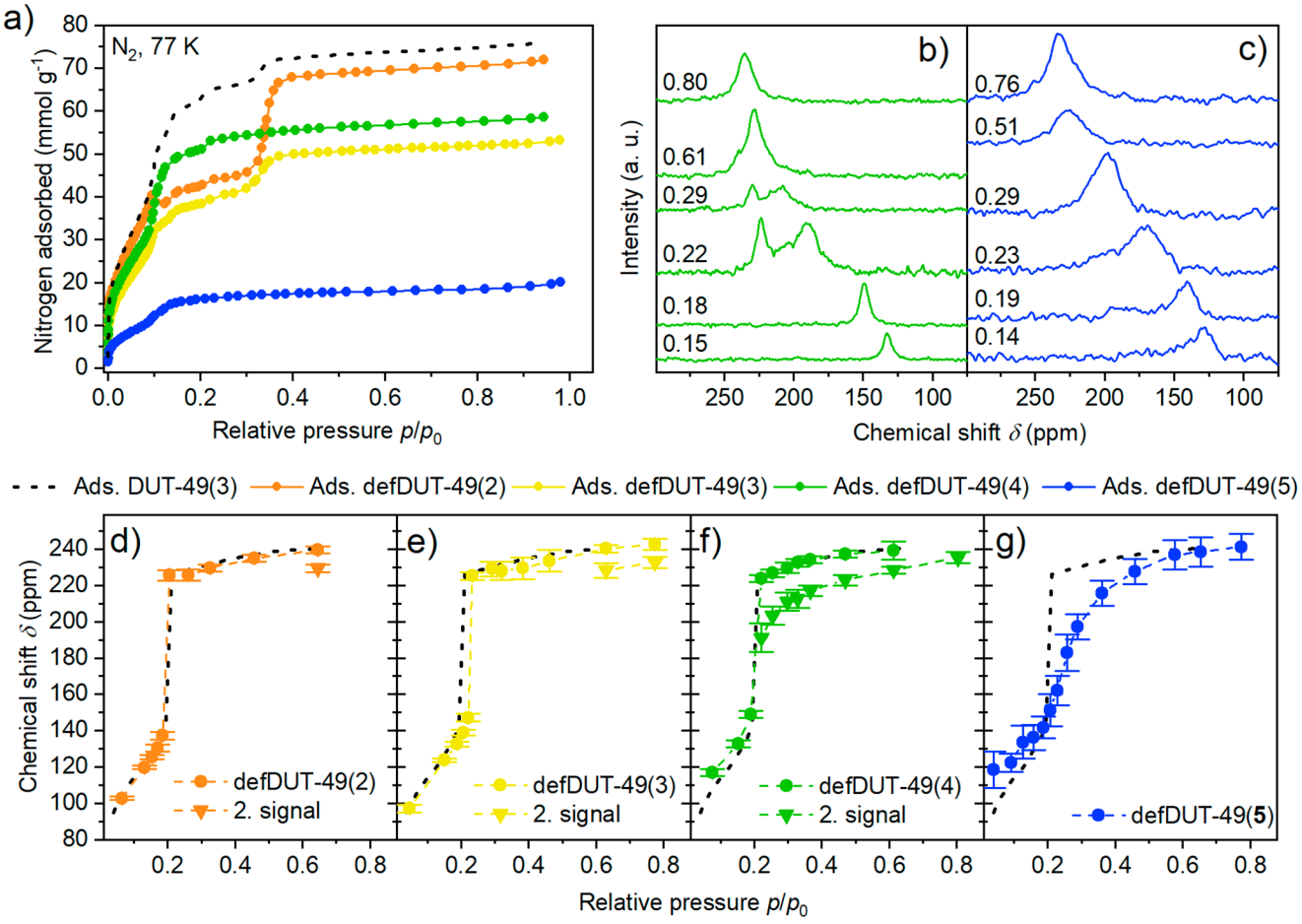

Figure 4. (a) Nitrogen adsorption isotherms at 77 K of selected samples. Selected ^{129}Xe NMR spectra of (b) defDUT-49(4) and (c) defDUT-49(5); relative pressures of Xe are given as numbers on the left of the spectra. Evolution of the chemical shift with increasing relative pressure upon adsorption for defDUT-49(2) (d, orange), defDUT-49(3) (e, yellow), defDUT-49(4) (f, green), and defDUT-49(5) (g, blue). Isotherm and chemical shifts of DUT-49(3) are provided as black dashed lines for comparison.

structural contraction are also expected to decrease to some extent with decreasing crystal size, which could explain the absence of structural contraction of DUT-49 samples with crystals smaller than 1 μm upon adsorption of nitrogen at 77 K.[33] In fact, pronounced changes of the chemical shift were also found to occur for samples with mean crystal size below 1 μm. The presence of NGA and structural contraction in all performed NMR experiments is a consequence of the higher adsorption enthalpy of xenon compared to nitrogen.[46] Thus, this finding complements recent computational analysis of crystal size effects in pillared-layer MOF systems in which the activation barrier for structural transition of the MOF crystal was found to increase with decreasing crystal size.[8,9] Both the decrease in adsorption-induced stress and the increase in activation barrier for structural transition support the experimentally observed absence of structural transitions in flexible MOFs.[10,14,33,47] *In situ* ^{129}Xe NMR experiments prove to be very sensitive in directly probing the interactions and mobility of the fluid within the crystals and pores of DUT-49, especially when the pores are saturated. This approach extends the previous analysis of crystals size effects in DUT-49 which focused on the adsorption behavior and structural transition of the solid.[21,33,35]

***In Situ* ^{129}Xe NMR Studies of Defect Effects.** The ^{129}Xe NMR unambiguously shows the decrease in chemical shift of adsorbate (and as consequence reduced overall Xe−solid interaction energy) for downsized crystals. The reasons for such observation can be the growing fraction of the outer surface, but the decrease in chemical shift might also potentially be caused by increased concentration of defects in the internal structure, which change the pore size and surface chemistry and thus reduce the average solid−fluid interactions.[12] In fact, crystal size engineering often involves auxiliary reagents. Rational engineering of MOFs with a high concentration of structurally defined defects has become a major field of research,[19] especially in Zr-based MOFs like UiO-66.[48] Modulators such as amino acids[49] and other monocarboxylic acids[13,49,50] are used in the synthesis to improve the crystallinity by taking part in the crystallization process in competition with the linker. Consequently, crystal seeding is reduced to yield larger crystals. However, in some cases, the modulator molecules are built in the backbone of the MOF, creating structural defects[17] often missing linkers[51] that can strongly impact the porosity. At higher defect concentrations, entire cluster−linker complexes are removed from the structure, creating larger mesopores[52] detectable by adsorption experiments[53] and usable for catalytic[54,55] and gas storage applications.[56] Interestingly DUT-49 and UiO-66, although very different in composition and porosity, both share the same **fcu** topology in which the 12-connecting Zr-cluster in UiO-66 represents the 12-connecting cuboctahedral MOP in DUT-49. These building blocks are arranged in a cubic close packing

https://dx.doi.org/10.1021/acs.chemmater.0c01059
Chem. Mater. 2020, 32, 4641−4650

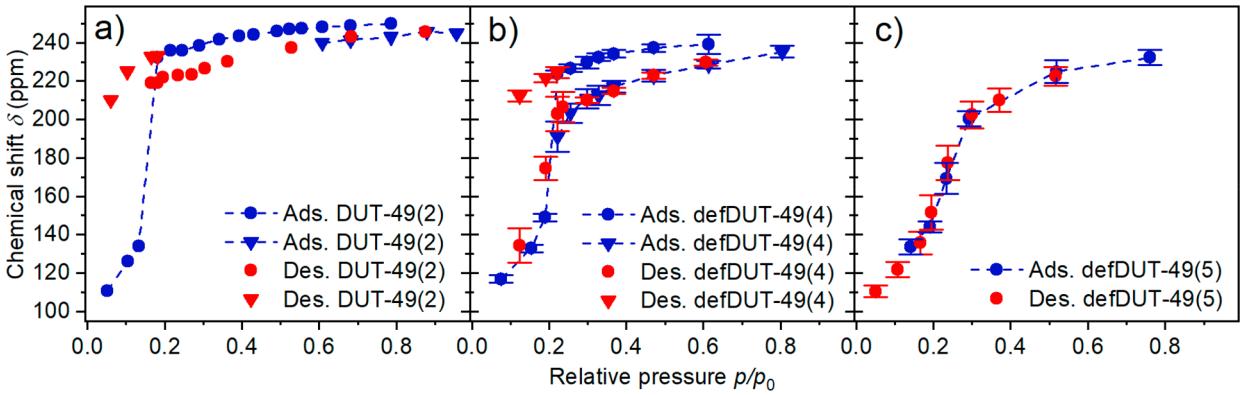

Figure 5. Adsorption (blue) and desorption (red) isotherms recorded by *in situ* ^{129}Xe NMR at 200 K on (a) DUT-49(2), (b) defDUT-49(4), and (c) defDUT-49(5). The appearance of a second signal is indicated by a triangle.

with tetrahedral and octahedral voids/pores. The introduction of modulating agent (in this case cdc) in the backbone of DUT-49 is thus expected to yield similar types of defects as reported for UiO-66-type MOFs.

To study the impact of defects in DUT-49 on the adsorption behavior, NGA, and fluid−solid interactions, the samples with targeted concentration of defects (defDUT-49(2), -(3), -(4), and -(5)) were analyzed by *in situ* ^{129}Xe NMR. From the nitrogen adsorption experiments at 77 K, it is obvious that the introduction of defects strongly influences the porosity of the resulting material. The obtained evolution of chemical shifts with increasing pressure was compared to the previously discussed isotherms of DUT-49(2) acting as nondefective reference with comparable crystal size distribution. The recorded isotherms of defDUT-49(2) and -(3) are found to be very similar (Figure 4). All three isotherms exhibit the same low-pressure chemical shift, structural contraction, and NGA at a relative pressure around 0.19. The appearance of a second signal at higher pressures indicates the pore opening. Consequently, the small number of defects does not impact the adsorption behavior. This finding is in line with the nitrogen physisorption isotherms at 77 K, in which all three samples exhibit hysteresis and NGA. However, higher defect concentration in defDUT-49(4) alters the adsorption behavior drastically. After structural contraction at a relative pressure of 0.2, a second signal in addition to the signal assigned to DUT-49*cp* is observed. This signal is found at chemical shifts ca. 20 ppm lower than the signal of DUT-49*cp* and is maintained over the whole pressure range. At higher pressures, the DUT-49*cp* signal disappears, and only one signal remains at a relative pressure of 0.8. This finding and the reduced chemical shift are indications that this second signal can be attributed to xenon adsorbed in DUT-49*op*. Consequently, only a part of the bulk material in defDUT-49(4) exhibits structural contraction, and the other part of the sample remains in the *op* phase. This is in line with the nitrogen adsorption isotherms which were found to be free of NGA, hysteresis, or other indications of a structural transition. The observed trend is supported by the analysis of defDUT-49(5). In this case, no signal for xenon adsorbed in the *cp* phase is detectable, which implies that the formation of DUT-49*cp* is completely suppressed over the whole pressure range. Interestingly, defDUT-49(4) and -(5) exhibit a higher chemical shift in the low-pressure region, indicating that the microporous structure of these samples is affected by the addition of cdc. This can be attributed to either a change in surface functionality or the collapse of mesopores with defective pore walls that introduce additional microporosity. To further analyze the phase mixture in defDUT-49(4) and to probe reversibility of the adsorption, additional desorption isotherms were recorded for defDUT-49(4) and -(5) and compared to the data recorded for DUT-49(2) (Figure 5). The sudden increase in chemical shift upon contraction during desorption and the corresponding hysteresis observed for DUT-49(2) are in stark contrast to the reversible isotherm of defDUT-49(5), which lacks hysteresis and any indication for structural contraction. On the other hand, defDUT-49(4) exhibits partial contraction during adsorption and desorption in which signals for DUT-49*op* and -*cp* could be detected at intermediate and low pressures, respectively. Consequently, the incorporation of 25% cdc in the DUT-49 framework seems to be the critical value to observe strong changes in adsorption behavior and structural transition. It has to be noted that the strong reduction in uptake indicated that the majority of the framework collapsed, and only small local regions in the bulk retained the porosity which is apparently altered by cdc incorporation and matrix effects. The complete suppression of *cp* formation in defDUT-49(5) with 50% cdc indicates that higher degrees of cdc inclusion impacts all particles within this particular material and strongly alters the adsorption behavior.

While variation of the crystal size demonstrated to impact the fluid−solid interaction, high concentration of defects seems to also impact the adsorption-induced contraction demonstrated by the absence of structural contraction in defDUT-49(5). The critical level of defects via cdc inclusion was found to be in the range beyond 45%, which is a surprisingly high level at which almost every fourth linear link between the MOPs is missing. In contrast, low defect concentrations do not impact the adsorption behavior, structural contraction, and NGA in DUT-49. Consequently, the previously discussed evolution of chemical shift of nanometer-sized crystals of DUT-49 does not originate from structural defects but represents the prevail influence of particle size phenomena that were found to impact the adsorption energetics by changes in residence time and average interactions of the fluid with the porous host. In addition, structural contraction behavior is only impacted at rather high concentrations of defects which are not expected for a synthesis in which no defect forming agent is applied. The performed xenon NMR experiments provide a unique experimental approach to analyze these effects regardless of the materials porosity and were found to be suitable for discriminating between effects

https://dx.doi.org/10.1021/acs.chemmater.0c01059
Chem. Mater. 2020, 32, 4641−4650

caused by defects and crystal size. To the best of our knowledge, this is the first time *in situ* ^{129}Xe NMR experiments have been applied in studying particle size and defect effects in flexible MOFs or other materials that undergo adsorption-induced contraction. Nevertheless, a more detailed investigation of surface effects that are expected to be enhanced upon crystal downsizing is required. We thus envision that this method can be applied in a rage of experimental investigations to further study a range of materials know to exhibit similar behavior as DUT-49. In addition, the analysis of defDUT-49(5) which exhibits low crystallinity shows that this method might also be useful for low- or noncrystalline solids like covalent organic framework and porous polymers know to swell upon adsorption.[57]

CONCLUSIONS

In conclusion, we demonstrate the influence of particle size and defects on the adsorption behavior of the flexible MOF DUT-49(Cu) and its negative gas adsorption behavior by *in situ* ^{129}Xe NMR experiments. We show that analysis of the chemical shift in different pressure regimes allows to probe the average solid−fluid interactions providing a local probe for the adsorption-induced structural transitions. With decreasing mean crystal size, the average solid−fluid interactions in the saturated pores are found to strongly decrease, minimizing the driving force for structural transitions in smaller crystals. To probe whether defects or crystal size phenomena are responsible for the observed behavior, we investigated a series of six DUT-49 samples with increasing defect concentrations. We find that for low defect concentrations below 20% cdc and comparable crystal size no detectable difference in adsorption behavior is observed. However, at higher concentrations of defects beyond 25% cdc, which are not expected to occur in regularly synthesized DUT-49 crystals, the adsorption behavior is strongly altered leading to the absence of structural contraction and NGA. Consequently, we derive that the behavior observed for smaller crystal sizes does not originate from defects but reflects the impact of crystal size phenomena on the adsorption behavior in DUT-49. With the results presented in this work, we hope to demonstrate that particle size effects have a large impact on the adsorption interactions not only in flexible MOFs but also porous solids in general and hope to motivate further investigations in this field. In addition, we point out the need to apply various methods to elucidate the nature and structure of defects in both large and small crystals of flexible MOFs and complement these with methods to characterize guest−host properties.

ASSOCIATED CONTENT

Supporting Information

The Supporting Information is available free of charge at https://pubs.acs.org/doi/10.1021/acs.chemmater.0c01059.

Experimental data for the characterization of defective DUT-49 samples as well as raw NMR spectra of the performed experiments (PDF)

Crystallograhic data of DUT-158 (CCDC 1983549) (CIF)

AUTHOR INFORMATION

Corresponding Authors

Simon Krause − *Department of Inorganic Chemistry, Technische Universität Dresden, 01062 Dresden, Germany; Centre for Systems Chemistry, Stratingh Institute for Chemistry, University of Groningen, 9747 AG Groningen, The Netherlands;* orcid.org/0000-0001-9504-8514; Email: simon.krause@rug.nl

Stefan Kaskel − *Department of Inorganic Chemistry, Technische Universität Dresden, 01062 Dresden, Germany;* orcid.org/0000-0003-4572-0303; Email: stefan.kaskel@tu-dresden.de

Eike Brunner − *Chair of Bioanalytical Chemistry, Technische Universität Dresden, 01062 Dresden, Germany;* orcid.org/0000-0003-3511-9899; Email: eike.brunner@tu-dresden.de

Authors

Florian S. Reuter − *Chair of Bioanalytical Chemistry, Technische Universität Dresden, 01062 Dresden, Germany*

Sebastian Ehrling − *Department of Inorganic Chemistry, Technische Universität Dresden, 01062 Dresden, Germany;* orcid.org/0000-0003-0949-4572

Volodymyr Bon − *Department of Inorganic Chemistry, Technische Universität Dresden, 01062 Dresden, Germany;* orcid.org/0000-0002-9851-5031

Irena Senkovska − *Department of Inorganic Chemistry, Technische Universität Dresden, 01062 Dresden, Germany;* orcid.org/0000-0001-7052-1029

Complete contact information is available at: https://pubs.acs.org/10.1021/acs.chemmater.0c01059

Author Contributions

S.K. performed synthesis and characterization of the MOF materials, F.S.R. performed the ^{129}Xe NMR measurements, S.E. performed SEM analysis, V.B. performed single crystal analysis, and S.K, I.S., E.B., and S.K. coordinated the project and wrote the manuscript. All authors discussed the results and contributed to the final manuscript. All authors have given approval to the final version of the manuscript.

Funding

This project has received funding from the European Research Council (ERC) under the European Union's Horizon 2020 research and innovation program (grant agreement no. 742743). Financial support from the Deutsche Forschungsgemeinschaft (Research Unit FOR 2433 "MOF-Switches") is gratefully acknowledged.

Notes

The authors declare no competing financial interest.

ACKNOWLEDGMENTS

S.K. acknowledges the support of the Alexander von Humboldt Foundation and thanks Felicitas Kolbe for support in data analysis.

ABBREVIATIONS

DUT-49, Dresden University of Technology No. 49; def, defective; H_2cdc, 9*H*-carbazole-3,6-dicarboxylic acid; H_4bbcdc, 9,9′-(1,1′-[biphenyl]-4,4′-diyl)[bis(9*H*-carbazole-3,6-dicarboxylic acid)].

REFERENCES

(1) Schneemann, A.; Bon, V.; Schwedler, I.; Senkovska, I.; Kaskel, S.; Fischer, R. A. Flexible metal-organic frameworks. *Chem. Soc. Rev.* **2014**, *43* (16), 6062−6096.

(2) Chang, Z.; Yang, D.-H.; Xu, J.; Hu, T.-L.; Bu, X.-H. Flexible Metal−Organic Frameworks: Recent Advances and Potential Applications. *Adv. Mater.* **2015**, *27* (36), 5432−5441.

(3) Freund, P.; Senkovska, I.; Kaskel, S. Switchable Conductive MOF−Nanocarbon Composite Coatings as Threshold Sensing Architectures. *ACS Appl. Mater. Interfaces* **2017**, *9* (50), 43782−43789.
(4) Mason, J. A.; Oktawiec, J.; Taylor, M. K.; Hudson, M. R.; Rodriguez, J.; Bachman, J. E.; Gonzalez, M. I.; Cervellino, A.; Guagliardi, A.; Brown, C. M.; Llewellyn, P. L.; Masciocchi, N.; Long, J. R. Methane storage in flexible metal−organic frameworks with intrinsic thermal management. *Nature* **2015**, *527*, 357.
(5) Li, L.; Krishna, R.; Wang, Y.; Yang, J.; Wang, X.; Li, J. Exploiting the gate opening effect in a flexible MOF for selective adsorption of propyne from C1/C2/C3 hydrocarbons. *J. Mater. Chem. A* **2016**, *4* (3), 751−755.
(6) Li, L.; Lin, R.-B.; Krishna, R.; Wang, X.; Li, B.; Wu, H.; Li, J.; Zhou, W.; Chen, B. Flexible−Robust Metal−Organic Framework for Efficient Removal of Propyne from Propylene. *J. Am. Chem. Soc.* **2017**, *139* (23), 7733−7736.
(7) Bon, V.; Brunner, E.; Pöppl, A.; Kaskel, S. Unraveling Structure and Dynamics in Porous Frameworks via Advanced In Situ Characterization Techniques. *Adv. Funct. Mater.* **2020**, 1907847.
(8) Rogge, S. M. J.; Waroquier, M.; Van Speybroeck, V. Unraveling the thermodynamic criteria for size-dependent spontaneous phase separation in soft porous crystals. *Nat. Commun.* **2019**, *10* (1), 4842.
(9) Keupp, J.; Schmid, R. Molecular Dynamics Simulations of the "Breathing" Phase Transformation of MOF Nanocrystallites. *Adv. Theory Simul.* **2019**, *2* (11), 1900117.
(10) Zhang, C.; Gee, J. A.; Sholl, D. S.; Lively, R. P. Crystal-Size-Dependent Structural Transitions in Nanoporous Crystals: Adsorption-Induced Transitions in ZIF-8. *J. Phys. Chem. C* **2014**, *118* (35), 20727−20733.
(11) Miura, H.; Bon, V.; Senkovska, I.; Ehrling, S.; Watanabe, S.; Ohba, M.; Kaskel, S. Tuning the gate-opening pressure and particle size distribution of the switchable metal−organic framework DUT-8(Ni) by controlled nucleation in a micromixer. *Dalton Trans.* **2017**, *46* (40), 14002−14011.
(12) Tanaka, S.; Fujita, K.; Miyake, Y.; Miyamoto, M.; Hasegawa, Y.; Makino, T.; Van der Perre, S.; Cousin Saint Remi, J.; Van Assche, T.; Baron, G. V.; Denayer, J. F. M. Adsorption and Diffusion Phenomena in Crystal Size Engineered ZIF-8 MOF. *J. Phys. Chem. C* **2015**, *119* (51), 28430−28439.
(13) Firth, F. C. N.; Cliffe, M. J.; Vulpe, D.; Aragones-Anglada, M.; Moghadam, P. Z.; Fairen-Jimenez, D.; Slater, B.; Grey, C. P. Engineering new defective phases of UiO family metal−organic frameworks with water. *J. Mater. Chem. A* **2019**, *7* (7), 7459−7469.
(14) Kavoosi, N.; Bon, V.; Senkovska, I.; Krause, S.; Atzori, C.; Bonino, F.; Pallmann, J.; Paasch, S.; Brunner, E.; Kaskel, S. Tailoring adsorption induced phase transitions in the pillared-layer type metal-organic framework DUT-8(Ni). *Dalton Trans.* **2017**, *46* (46), 4685−4695.
(15) Linder-Patton, O. M.; Bloch, W. M.; Coghlan, C. J.; Sumida, K.; Kitagawa, S.; Furukawa, S.; Doonan, C. J.; Sumby, C. J. Particle size effects in the kinetic trapping of a structurally-locked form of a flexible MOF. *CrystEngComm* **2016**, *18* (22), 4172−4179.
(16) Cheetham, A. K.; Bennett, T. D.; Coudert, F.-X.; Goodwin, A. L. Defects and disorder in metal organic frameworks. *Dalton Trans.* **2016**, *45* (10), 4113−4126.
(17) Øien, S.; Wragg, D.; Reinsch, H.; Svelle, S.; Bordiga, S.; Lamberti, C.; Lillerud, K. P. Detailed Structure Analysis of Atomic Positions and Defects in Zirconium Metal−Organic Frameworks. *Cryst. Growth Des.* **2014**, *14* (11), 5370−5372.
(18) Morris, W.; Wang, S.; Cho, D.; Auyeung, E.; Li, P.; Farha, O. K.; Mirkin, C. A. Role of Modulators in Controlling the Colloidal Stability and Polydispersity of the UiO-66 Metal−Organic Framework. *ACS Appl. Mater. Interfaces* **2017**, *9* (39), 33413−33418.
(19) Fang, Z.; Bueken, B.; De Vos, D. E.; Fischer, R. A. Defect-Engineered Metal−Organic Frameworks. *Angew. Chem., Int. Ed.* **2015**, *54* (25), 7234−7254.
(20) Shang, W.; Kang, X.; Ning, H.; Zhang, J.; Zhang, X.; Wu, Z.; Mo, G.; Xing, X.; Han, B. Shape and Size Controlled Synthesis of MOF Nanocrystals with the Assistance of Ionic Liquid Mircoemulsions. *Langmuir* **2013**, *29* (43), 13168−13174.
(21) Krause, S.; Bon, V.; Senkovska, I.; Stoeck, U.; Wallacher, D.; Többens, D. M.; Zander, S.; Pillai, R. S.; Maurin, G.; Coudert, F.-X.; Kaskel, S. A pressure-amplifying framework material with negative gas adsorption transitions. *Nature* **2016**, *532* (7599), 348−352.
(22) Evans, J. D.; Bocquet, L.; Coudert, F.-X. Origins of Negative Gas Adsorption. *Chem.* **2016**, *1* (6), 873−886.
(23) Trepte, K.; Schaber, J.; Schwalbe, S.; Drache, F.; Senkovska, I.; Kaskel, S.; Kortus, J.; Brunner, E.; Seifert, G. The origin of the measured chemical shift of ^{129}Xe in UiO-66 and UiO-67 revealed by DFT investigations. *Phys. Chem. Chem. Phys.* **2017**, *19* (15), 10020−10027.
(24) Hoffmann, H. C.; Assfour, B.; Epperlein, F.; Klein, N.; Paasch, S.; Senkovska, I.; Kaskel, S.; Seifert, G.; Brunner, E. High-Pressure in Situ ^{129}Xe NMR Spectroscopy and Computer Simulations of Breathing Transitions in the Metal−Organic Framework Ni_2(2,6-ndc)$_2$(dabco) (DUT-8(Ni). *J. Am. Chem. Soc.* **2011**, *133*, 8681.
(25) Kolbe, F.; Krause, S.; Bon, V.; Senkovska, I.; Kaskel, S.; Brunner, E. High-Pressure in Situ 129Xe NMR Spectroscopy: Insights into Switching Mechanisms of Flexible Metal−Organic Frameworks Isoreticular to DUT-49. *Chem. Mater.* **2019**, *31* (16), 6193−6201.
(26) Oschatz, M.; Hoffmann, H. C.; Pallmann, J.; Schaber, J.; Borchardt, L.; Nickel, W.; Senkovska, I.; Rico-Francés, S.; Silvestre-Albero, J.; Kaskel, S.; Brunner, E. Structural Characterization of Micro- and Mesoporous Carbon Materials Using In Situ High Pressure 129Xe NMR Spectroscopy. *Chem. Mater.* **2014**, *26* (10), 3280−3288.
(27) Weber, J.; Schmidt, J.; Thomas, A.; Böhlmann, W. Micropore Analysis of Polymer Networks by Gas Sorption and ^{129}Xe NMR Spectroscopy: Toward a Better Understanding of Intrinsic Microporosity. *Langmuir* **2010**, *26* (19), 15650−15656.
(28) Ito, T.; Fraissard, J. ^{129}Xe NMR Study of Xenon Adsorbed on Y Zeolites. *J. Chem. Phys.* **1982**, *76*, 5225.
(29) Fraissard, J.; Ito, T. ^{129}Xe NMR Study of Adsorbed Xenon: A New Method for Studying Zeolites and Metal-Zeolites. *Zeolites* **1988**, *8*, 350.
(30) Jameson, C. J.; Jameson, A. K.; Gerald, R. E.; Lim, H.-M. Anisotropic Xe Chemical Shifts in Zeolites. The Role of Intra- and Intercrystallite Diffusion. *J. Phys. Chem. B* **1997**, *101* (42), 8418−8437.
(31) Schaber, J.; Krause, S.; Paasch, S.; Senkovska, I.; Bon, V.; Többens, D. M.; Wallacher, D.; Kaskel, S.; Brunner, E. In Situ Monitoring of Unique Switching Transitions in the Pressure-Amplifying Flexible Framework Material DUT-49 by High-Pressure 129Xe NMR Spectroscopy. *J. Phys. Chem. C* **2017**, *121* (9), 5195−5200.
(32) Demarquay, J.; Fraissard, J. ^{129}Xe NMR of Xenon Adsorbed on Zeolites: Relationship Between the Chemical Shift and the Void Space. *Chem. Phys. Lett.* **1987**, *136*, 314.
(33) Krause, S.; Bon, V.; Senkovska, I.; Többens, D. M.; Wallacher, D.; Pillai, R. S.; Maurin, G.; Kaskel, S. The effect of crystallite size on pressure amplification in switchable porous solids. *Nat. Commun.* **2018**, *9* (1), 1573.
(34) Stoeck, U.; Krause, S.; Bon, V.; Senkovska, I.; Kaskel, S. A highly porous metal-organic framework, constructed from a cuboctahedral super-molecular building block, with exceptionally high methane uptake. *Chem. Commun.* **2012**, *48* (88), 10841−10843.
(35) Krause, S.; Evans, J. D.; Bon, V.; Senkovska, I.; Ehrling, S.; Stoeck, U.; Yot, P. G.; Iacomi, P.; Llewellyn, P.; Maurin, G.; Coudert, F.-X.; Kaskel, S. Adsorption Contraction Mechanics: Understanding Breathing Energetics in Isoreticular Metal−Organic Frameworks. *J. Phys. Chem. C* **2018**, *122* (33), 19171−19179.
(36) Schindelin, J.; Arganda-Carreras, I.; Frise, E.; Kaynig, V.; Longair, M.; Pietzsch, T.; Preibisch, S.; Rueden, C.; Saalfeld, S.; Schmid, B.; Tinevez, J.-Y.; White, D. J.; Hartenstein, V.; Eliceiri, K.; Tomancak, P.; Cardona, A. Fiji: an open-source platform for biological-image analysis. *Nat. Methods* **2012**, *9* (7), 676−682.

https://dx.doi.org/10.1021/acs.chemmater.0c01059
Chem. Mater. 2020, 32, 4641−4650

(37) Raiford, D. S.; Fisk, C. L.; Becker, E. D. Calibration of methanol and ethylene glycol nuclear magnetic resonance thermometers. *Anal. Chem.* **1979**, *51* (12), 2050−2051.
(38) Van Geet, A. L. Calibration of methanol nuclear magnetic resonance thermometer at low temperature. *Anal. Chem.* **1970**, *42* (6), 679−680.
(39) Lifshits, L. M.; Zeller, M.; Campana, C. F.; Klosterman, J. K. Metal−Organic Frameworks as Supramolecular Templates for Directing Aromatic Packing Motifs. *Cryst. Growth Des.* **2017**, *17* (10), 5449−5457.
(40) Dissegna, S.; Vervoorts, P.; Hobday, C. L.; Düren, T.; Daisenberger, D.; Smith, A. J.; Fischer, R. A.; Kieslich, G. Tuning the Mechanical Response of Metal−Organic Frameworks by Defect Engineering. *J. Am. Chem. Soc.* **2018**, *140* (37), 11581−11584.
(41) Zheng, B.; Fu, F.; Wang, L. L.; Wang, J.; Du, L.; Du, H. Effect of Defects on the Mechanical Deformation Mechanisms of Metal−Organic Framework-5: A Molecular Dynamics Investigation. *J. Phys. Chem. C* **2018**, *122* (8), 4300−4306.
(42) Garai, B.; Bon, V.; Krause, S.; Schwotzer, F.; Gerlach, M.; Senkovska, I.; Kaskel, S. Tunable Flexibility and Porosity of the Metal−Organic Framework DUT-49 through Postsynthetic Metal Exchange. *Chem. Mater.* **2020**, *32* (2), 889−896.
(43) Jameson, C. J.; Jameson, A. K.; Cohen, S. M. Temperature and density dependence of ^{129}Xe chemical shift in xenon gas. *J. Chem. Phys.* **1973**, *59* (8), 4540−4546.
(44) Mair, R. W.; Rosen, M. S.; Wang, R.; Cory, D. G.; Walsworth, R. L. Diffusion NMR methods applied to xenon gas for materials study. *Magn. Reson. Chem.* **2002**, *40* (13), S29−S39.
(45) Krause, S.; Bon, V.; Du, H.; Dunin-Borkowski, R. E.; Stoeck, U.; Senkovska, I.; Kaskel, S. The impact of crystal size and temperature on the adsorption-induced flexibility of the Zr-based metal-organic framework DUT-98. *Beilstein J. Nanotechnol.* **2019**, *10*, 1737−1744.
(46) Boutin, A.; Springuel-Huet, M.-A.; Nossov, A.; Gédéon, A.; Loiseau, T.; Volkringer, C.; Férey, G.; Coudert, F.-X.; Fuchs, A. H. Breathing Transitions in MIL-53(Al) Metal−Organic Framework Upon Xenon Adsorption. *Angew. Chem., Int. Ed.* **2009**, *48* (44), 8314−8317.
(47) Ehrling, S.; Senkovska, I.; Bon, V.; Evans, J. D.; Petkov, P.; Krupskaya, Y.; Kataev, V.; Wulf, T.; Krylov, A.; Vtyurin, A.; Krylova, S.; Adichtchev, S.; Slyusareva, E.; Weiss, M. S.; Büchner, B.; Heine, T.; Kaskel, S. Crystal size versus paddle wheel deformability: selective gated adsorption transitions of the switchable metal−organic frameworks DUT-8(Co) and DUT-8(Ni). *J. Mater. Chem. A* **2019**, *7* (37), 21459−21475.
(48) Cavka, J. H.; Jakobsen, S.; Olsbye, U.; Guillou, N.; Lamberti, C.; Bordiga, S.; Lillerud, K. P. A New Zirconium Inorganic Building Brick Forming Metal Organic Frameworks with Exceptional Stability. *J. Am. Chem. Soc.* **2008**, *130* (42), 13850−13851.
(49) Marshall, R. J.; Hobday, C. L.; Murphie, C. F.; Griffin, S. L.; Morrison, C. A.; Moggach, S. A.; Forgan, R. S. Amino acids as highly efficient modulators for single crystals of zirconium and hafnium metal−organic frameworks. *J. Mater. Chem. A* **2016**, *4* (18), 6955−6963.
(50) Atzori, C.; Shearer, G. C.; Maschio, L.; Civalleri, B.; Bonino, F.; Lamberti, C.; Svelle, S.; Lillerud, K. P.; Bordiga, S. Effect of Benzoic Acid as a Modulator in the Structure of UiO-66: An Experimental and Computational Study. *J. Phys. Chem. C* **2017**, *121* (17), 9312−9324.
(51) Driscoll, D. M.; Troya, D.; Usov, P. M.; Maynes, A. J.; Morris, A. J.; Morris, J. R. Characterization of Undercoordinated Zr Defect Sites in UiO-66 with Vibrational Spectroscopy of Adsorbed CO. *J. Phys. Chem. C* **2018**, *122* (26), 14582−14589.
(52) Cliffe, M. J.; Wan, W.; Zou, X.; Chater, P. A.; Kleppe, A. K.; Tucker, M. G.; Wilhelm, H.; Funnell, N. P.; Coudert, F.-X.; Goodwin, A. L. Correlated defect nanoregions in a metal−organic framework. *Nat. Commun.* **2014**, *5*, 4176.
(53) Huang, H.; Li, J.-R.; Wang, K.; Han, T.; Tong, M.; Li, L.; Xie, Y.; Yang, Q.; Liu, D.; Zhong, C. An in situ self-assembly template strategy for the preparation of hierarchical-pore metal-organic frameworks. *Nat. Commun.* **2015**, *6*, 8847.
(54) Liu, T.; Liu, Y.; Yao, L.; Yang, W.; Tian, L.; Liu, H.; Liu, D.; Wang, C. Controllable formation of meso- and macropores within metal−organic framework crystals via a citric acid modulator. *Nanoscale* **2018**, *10* (27), 13194−13201.
(55) Mautschke, H. H.; Drache, F.; Senkovska, I.; Kaskel, S.; Llabrés i Xamena, F. X. Catalytic properties of pristine and defect-engineered Zr-MOF-808 metal organic frameworks. *Catal. Sci. Technol.* **2018**, *8* (14), 3610−3616.
(56) Yuan, S.; Zou, L.; Qin, J.-S.; Li, J.; Huang, L.; Feng, L.; Wang, X.; Bosch, M.; Alsalme, A.; Cagin, T.; Zhou, H.-C. Construction of hierarchically porous metal−organic frameworks through linker labilization. *Nat. Commun.* **2017**, *8*, 15356.
(57) Hart, K. E.; Springmeier, J. M.; McKeown, N. B.; Colina, C. M. Simulated swelling during low-temperature N_2 adsorption in polymers of intrinsic microporosity. *Phys. Chem. Chem. Phys.* **2013**, *15* (46), 20161−20169.

https://dx.doi.org/10.1021/acs.chemmater.0c01059
Chem. Mater. 2020, 32, 4641−4650